Journal of Thermal Analysis and Calorimetry
https://doi.org/10.1007/s10973-024-12891-5

Porous polypropylene produced by phase separation for high solar reflectivity and passive cooling

Csenge Vámos[1,2] · Tamás Bárány[1,3] · Botond Béla Marosfői[2]

Received: 31 August 2023 / Accepted: 9 January 2024

Abstract

Passive cooling techniques have gained widespread use in everyday life and various industries by utilizing sunlight reflection to cool objects without requiring additional energy input. Porous polymer materials possess the unique ability to provide both thermal insulation and solar reflection due to their inherent multiphase structure. In this study, we developed a porous polypropylene (PP) with a hierarchically structured surface layer using a simple and efficient solvent treatment method based on recrystallization. As a result, the porous structure and hierarchically structured surface significantly increase the solar reflectance from 11 to 86%. We found that by manipulating the recrystallization process and using reflective additives, solar reflectivity can be further improved. With the use of TiO_2 and $BaSO_4$ additives, a solar reflectance of 90% was achieved, while a solar reflectance of 93% was achieved with nucleating agents. In practical terms, these improvements result in significant temperature reductions in cooling performance tests compared to extruded PP sheets: 17, 19, and 22 °C for porous PP, porous PP/TiO_2 or PP/$BaSO_4$, and porous nucleated PP, respectively. The modification method introduced could help PP offer new possibilities for developing low-cost chemically resistant and thermally insulating layers in thermal management applications.

Keywords Passive cooling material · Hierarchical porous layer · Solar reflectance · Thermal insulation · Polypropylene

Introduction

Lately, energy-saving, CO_2 emission, and environmental footprint reduction have become key expressions as climatic changes are undoubtedly related to human industrial activity. The industrial and residential building sectors consume significant amounts of electric energy. Moreover, increasing demands and improving living standards in developed and developing countries create additional energy consumption, partly because of the widespread use of air conditioning [1, 2]. Much of the energy used in buildings, approximately 40%, is used for cooling or heating [3]. Therefore, it is important to create sustainable methods like passive cooling techniques to counteract the increase in the temperature of buildings. These methods help keep a desirable level of comfort while minimizing energy consumption. Lately, there has been a notable interest in passive cooling techniques, particularly heat and solar-reflective techniques. These methods have significant appeal due to their economic viability, making them suitable for buildings in developing countries. Heat and solar-reflective techniques help to reduce most of the direct solar heat gain inside the building [4]. Also, the energy consumption of air conditioners could be reduced considerably if more incoming solar radiation could be reflected from the walls. As part of this endeavor, technologists work on developing materials with reflective and thermal insulation properties in the whole solar spectrum, which could effectively reduce energy demand [5].

About 5% of the energy of solar radiation is in the ultraviolet band (UV) (200–400 nm), 43% in the visible band (VIS) (400–800 nm), and 52% in the near-infrared band

✉ Csenge Vámos
csenge.vamos@furukawaelectric.com

Tamás Bárány
barany@pt.bme.hu

Botond Béla Marosfői
botond.marosfoi@furukawaelectric.com

[1] Department of Polymer Engineering, Faculty of Mechanical Engineering, Budapest University of Technology and Economics, Műegyetem rkp. 3, Budapest 1111, Hungary

[2] Furukawa Electric Institute of Technology Ltd, Késmárk u. 28/A, 1158 Budapest, Hungary

[3] MTA-BME Lendület Lightweight Polymer Composites Research Group, Műegyetem rkp. 3, 1111 Budapest, Hungary

Published online: 24 February 2024

(NIR) (800–2500 nm), therefore it is important to improve reflectivity in all these bands to increase the efficiency of solar reflectivity [6, 7]. Usually, the reflectivity of products can be evaluated with total solar reflectance (TSR). TSR shows the amount of the energy of incident sunlight reflected from the surface. Higher TSR means better reflectivity and higher thermal insulation in the range of 200 to 2500 nm [6].

In general, effective strategies can serve as a basis for producing solar-reflective polymer materials: adding optically active additives to the polymer matrix [8, 9] and creating porous polymers [10–12]. In each case, the solar reflectivity and thus the thermal insulation of the polymer is determined based on the fluctuation of the refractive index at the interface of the two materials [13, 14]. Reflective additives, such as titanium dioxide (TiO_2), barium sulfate ($BaSO_4$), and zinc dioxide (ZnO) are widely used in the fabrication of polymer composites with enhanced solar reflectivity [8, 12]. Numerous factors have been investigated, such as the size, amount and distribution of particles in the polymer matrix [15–17]. For example, the diameter of the particles greatly determines the intensity and directional distribution of scattered light. In accordance with Fresnel's rules, particle size should be at least half the wavelength of incident light to be scattered [13]. Commercially available TiO_2 pigments are one of the most effective additives to reflect visible light, as their particle size distribution is optimized within the range of 200 to 300 nm [18]. However, their near-infrared reflectance remains quite moderate [19]. In order to increase the reflective ability of TiO_2 in the whole solar spectrum, multiple particle sizes are considered because the wider the size distribution of the particles, the wider the spectrum they can reflect [20]. The uniform distribution of these particles within the matrix is desirable but sometimes the particles aggregate, which can limit their light-scattering efficiency. Various strategies have been proposed for this problem, including extenders or dispersants, and also polymer-encapsulated particles [8, 17]. However, it is still a challenging task to achieve homogeneous optical properties with an even distribution of particles in the polymer matrix.

For years, conventional applications have been dominated by scattering systems utilizing inorganic nanoparticles. However, porous polymers are attracting more and more attention due to their cost-effectiveness, ease of preparation, and wide availability. In recent times, there has been a surge in research interest toward solar-reflective porous polymer materials, owing to their promising structure, which enhances material cooling properties [21]. During the production of light-scattering polymers, we utilize the refractive index differences between the air voids and the polymer matrix [22, 23]. In the case of porous light-scattering polymers, there are concerns regarding broad solar reflectivity since the light scattering of such porous polymers depends on the morphology of the porous structure. It is advisable to foam a porous structure with a certain degree of anisotropy in the out-of-plane direction [24, 25]. The morphology of porous polymers can be tailored through different fabrication methods, including microcellular foaming [26, 27], electrospinning [27], and phase separation [28, 29], etc.

Among them, phase separation-based techniques, like thermally induced phase separation (TIPS) are among the most popular methods to produce porous polymers. TIPS is compatible with a wide range of amorphous or semicrystalline polymers. In a typical process of TIPS, the polymer is dissolved into a solvent at an elevated temperature, which produces a homogeneous mixture. It is followed by cooling the mixture, which initiates the phase separations. Finally, the polymer microporous films are obtained after the diluent is extracted completely [30]. With this method, an anisotropic porous structure can be created, which provides high scattering ability in the whole solar spectrum [31, 32].

PP is one of the fastest-growing and most widely used commodity polymers and its crystalline structure and properties can be manipulated within a wide range [33]. PP, a semicrystalline polymer, appears translucent or opaque because it contains structural heterogeneities (so-called spherulites) that scatter light. Nowadays, PP is widely used in the packaging industry and microporous membrane technology, where nucleating agents are frequently used to alter the distribution and size of spherulites. The visible light scattering of the product can be reduced with nucleating agents in the packaging industry, and pore size and its distribution can be fine-tuned in the production of polymer membranes, since large nucleus density can be reached with nucleating agents [34–36]. However, our knowledge regarding the optical activity of hierarchical porous PP structures produced by phase separation is limited. The synergistic effect of reflective materials and porous structure, or harnessing the ability of the nucleating agents to modify the pore structure can enhance the light-scattering ability of porous PP. This dual approach is not only promising for amplifying light-scattering efficiency but also paves the way for novel applications.

In our previous study, we introduced a novel solvent treatment method based on phase separation. Due to the layer created with micro- and nanoscale patterns on an extruded PP sheet, a water contact angle of more than 160° was measured [37, 38].

In this study, we demonstrate that solar reflective, porous PP surface layers can be constructed from PP sheets by solvent treatment. We compared the solar-reflective

performance and thermal insulation ability of porous PP, porous PP composites, and porous nucleated PP. We investigated the combined effect of the structure of the porous layer, the presence of optical additives and the nucleating agent on both the structure and properties of PP sheets by scanning electron microscopy (SEM), spectrophotometry, and porosimeter and cooling test. The cooling performance of samples was evaluated with a laboratory-based simplified sun test.

Experimental

Materials

The polypropylene was Tipplen H681F extrusion grade homopolymer (MOL Petrochemicals, Tiszaújváros, Hungary). The reflective additives were $BaSO_4$ with 98% purity supplied by Thermo Scientific, Belgium and TiO_2, KTR 600 with 98% of the particles below 45 µm (Koltex Color s.r.o, Mnichovo Hradiště, Czech Republic). Both the $BaSO_4$ and TiO_2 were added to the polypropylene in amounts of 5, 10, and 20 mass%. The nucleating agent was ADK STAB NA-21E (Adeka, Tokyo, Japan). It was added to the polymer in the amount of 500 ppm.

Sample preparation

We prepared 1 mm thick PP/$BaSO_4$ and PP/TiO_2 sheets and nucleated samples with 500 ppm in two extrusion steps. For the production of the masterbatches of PP/$BaSO_4$ and PP/TiO_2 with 30 mass% and a masterbatch of nucleated PP with in one line1 mass%, the additive powders and PP pellets were dry-mixed in advance and extruded with a co-rotating twin-screw extruder (Brabender Plasti-Corder, Duisburg, Germany, features: L/D ratio: 19, screw diameter: 20 mm), with a rod die. The temperature zones were set to 190, 200, 200, 200, and 200 °C from hopper to die. The temperature of the die was 200 °C, and screw speed was 20 L min^{-1}. The extruded masterbatch filaments were pelletized with an S330 granulator (Rapid, Bredaryd, Sweden) and added to the PP pellets.

Fig. 1 The arrangement of laboratory-scaled "sun test"

We extruded 1-mm thick sheets using the previously prepared masterbatches with a twin-screw TSA extruder (Cernobbio, Italy, features: L/D ratio: 40, screw diameter: 32 mm) and a wide-gap die. The width of the die was 250 mm, and the gap size was set to 1.1 mm. The temperature profile of the extruder in the direction of the melt flow was as follows: 200, 200, 195, and 190 °C. The temperature of the die over the entire width was 190 °C, dosage was in one line 6 kg h^{-1}, and the rotational speed of the screw was 60 rpm. The temperature of the Trocellen QCAL-Quadro Calandra Linea R&D-OG calender used for drawing was 30 °C.

The samples were solvent-treated with xylene (mixture of isomers, purity 98%, VWR Chemicals, Germany), which was used as received. The samples were immersed into xylene at 125 °C for 60, 120, and 180 s and dried at 30 °C for 24 h in an air-ventilated oven (UT6120, Thermo Fisher Scientific, USA), then 24 h in a vacuum oven (FCD-3000, Faithful) at 30 °C.

Sample testing

Surface and cross-section morphology were analyzed with a Jeol JSM-IT 200 scanning electron microscope (SEM). For the examination of cross-sectional morphology, samples were cryo-fractured and sputtered with a thin gold layer for 50 s at 10 mA in a vacuum before SEM imaging.

The melting and crystallization behavior of the samples were conducted in a differential scanning calorimetry (DSC Q2000; TA Instruments, New Castle, USA). The DSC samples were first heated from 30 to 220 °C at 10 °C min^{-1}. This temperature was maintained for 5 min to eliminate thermal history, then the samples were cooled to 30 °C at a rate of 10 °C min^{-1}. The degree of crystallinity (X_c) was calculated with Eq. (1):

$$X_c = \left(\frac{\Delta H_m}{\Delta H_0}\right) \times 100 \quad (1)$$

where ΔH_m and ΔH_0 are the first melting enthalpy and melting enthalpy of a 100% crystalline sample (for PP it is 207 J g^{-1} [39]).

The porosity was determined from the true and apparent density according to Eq. (2):

$$\varepsilon(\%) = \left(\frac{\rho_t - \rho_a}{\rho_t}\right) * 100 \quad (2)$$

where ε is the porosity, and ρ_t and ρ_a are the true and apparent density of the samples, respectively.

ρ_a was determined from 4 cm × 4 cm samples. We removed the skin layer from both sides of the treated samples and measured their mass. ρ_a is obtained by dividing the mass of the samples by their volume. ρ_t was measured on an Ultra pycnometer 1000 (Quantachrome, Boynton Beach, FL, USA) with helium at 20 °C.

We used a PerkinElmer 1050 spectrometer for the reflectance measurements. For the diffuse reflectance measurements, the specular mirror output of the PerkinElmer 150 mm integrating sphere was removed so only the diffuse part of the reflected light was measured. We also performed the total reflectance measurement with a closed integrating sphere to register the total reflected light. In both cases, the measurement was carried out in the wavelength range of 200–2500 nm, with a resolution of 10 nm.

To determine thermal insulation properties, the area under the reflection spectra obtained during spectrophotometry is characterized with the TSR index. This indicates the reflected percentage of solar radiation. For the TSR index, the spectral distribution of solar radiation must also be taken into account. To measure the amount of reflected solar radiation, we have to examine each range. In the examined wavelength range of 200–2500 nm, the total energy of solar radiation is 892.2873 W m^{-2}. The value of the TSR index can be determined with Eq. (3) [6].

$$TSR(\%) = \frac{\int (R[\%] * I(\lambda) d\lambda)}{\int I(\lambda) d\lambda} * 100 \quad (3)$$

We tested the samples as heat-reflective surfaces under laboratory conditions using the so-called sun test. In the tests, the upper side of two boxes (80 × 80x80 mm) was covered with the samples to be tested. The boxes were illuminated from above with a 150 W light bulb, whose spectral distribution is similar to that of the sun. The distance between the light bulb and the boxes was 400 mm. Two temperature sensors were set at the same height (40 mm) in both boxes. The reference sample, an extruded polypropylene sheet, was always placed on one of the two boxes. We chose the duration of the tests in such a way that the temperature inside the boxes could stabilize in all cases. During evaluation, we plotted the temperature difference (ΔT) between the two boxes as a function of time. Figure 1 shows the layout of the test.

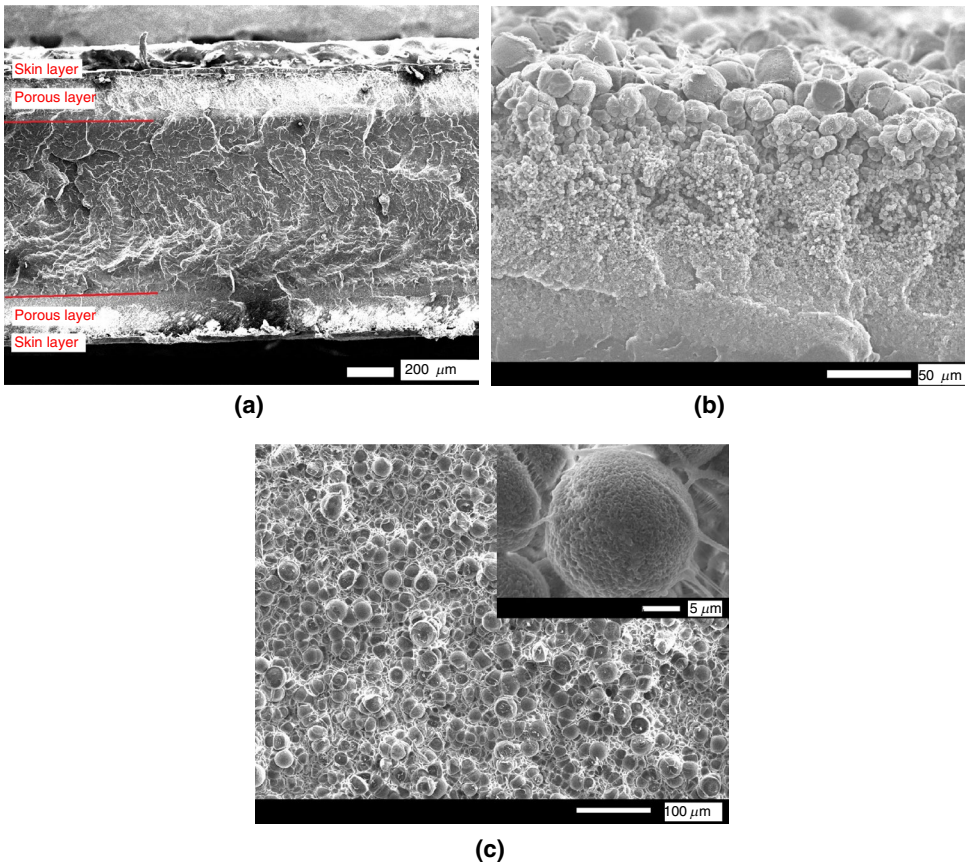

Fig. 2 SEM images of **a** cross-sectional area of solvent-treated PP sheet with a porous surface layer and skin layer, **b** SEM image of a porous layer produced with higher magnification **c** top-view SEM image of a solvent-treated PP sheet. The applied solvent treatment was 125 °C, 60 s

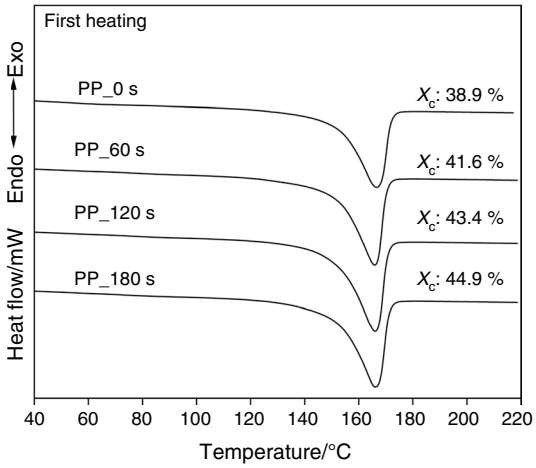

Fig. 3 First melting curves of solvent-treated PP sheets

Table 1 Characteristics of solvent-treated PP sheets; the applied solvent temperature was 125 °C

Immersion time/s	Porous layer thickness/µm	Porosity/%
0	–	–
60	133.4	19
120	174.9	24
180	220.4	28

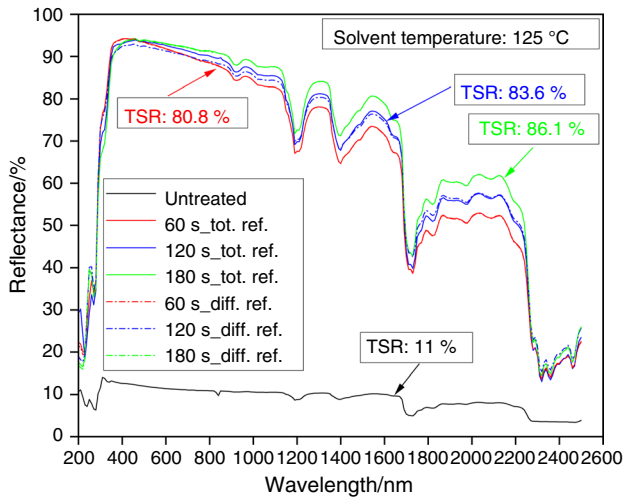

Fig. 4 Total and diffuse reflectance of solvent-treated PP sheets after different immersion times (60, 120, 180 s) compared to the untreated sample

Results

The effect of the porous surface layer on solar reflectance

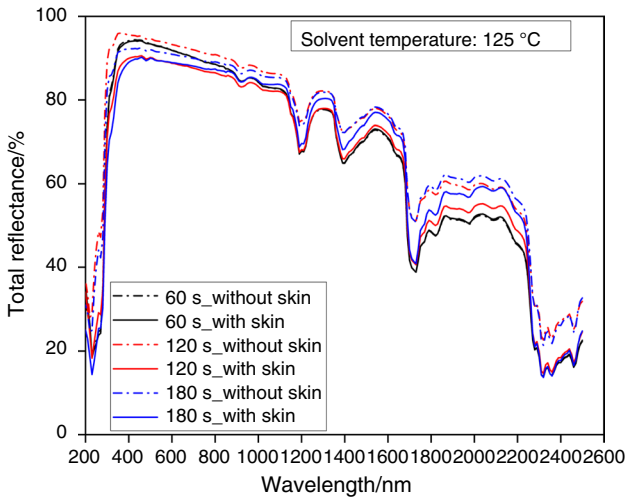

Fig. 5 Total reflectance of solvent-treated PP sheets with and without the skin layer

Preliminary studies revealed several morphological changes on the surface layer of the PP sheets after the solvent treatment. The surface structure of the solvent-treated samples was examined by SEM and is presented in overview images (Fig. 2).

The solvent swells the surface region in several tens of micrometers depth, increasing chain mobility. When the solvent evaporates, recrystallization takes place, leading to the formation of loosely attached spherulites. In addition to the porous layer on the surface of the sample, another compact structure also appears on top of the porous structure, the "skin layer", which can be peeled off the treated PP sheets. It is also noticeable that the structure of the porous layer is anisotropic. The cross-sectional view with larger magnification indicates that the spherulites are larger close to the surface than the spherulites in deeper layers of the porous structure.

The enlarged SEM image of a single spherulite reveals that the surface of spherulites has nano-roughness, which also contributes to the enhanced broad solar reflectivity. The broad size distribution of spherulites in the cross-section, as they play the role of scattering centers, and the further roughness of their surfaces indicate that hierarchically structured porous layers can have high solar reflectance in a wide wavelength range [7, 40]. The melting curves of solvent-treated samples with different immersion times are shown in Fig. 3.

The effect of recrystallization on structural changes is clearly visible in Fig. 3. X_c becomes monotonously larger as immersion time increases. The untreated, extruded PP sample shows an X_c of 38.9%, and the X_c of solvent-treated PP samples reaches 41.6, 43.4, and 44.9%, which can be attributed to greater crystallinity in the solvent-affected layer. As

solvent treatment time is increased, the thickness ratio of the solvent-affected layer and the bulk phase increases as well, leading to the overall increment in X_c.

Table 1 shows the effect of recrystallization in the solvent-affected layer on the porosity and porous layer thickness of the solvent-treated samples subjected to different solvent immersion times.

The thickness of the porous layer and the porosity of solvent-treated PP sheets increase with immersion time as well. These results show that longer immersion time results in the greater crystallinity, and thicker and more porous structure of the solvent-treated samples, which agrees well with the literature [30, 41].

All these structural modifications have a great impact on light reflection. This change is demonstrated by Fig. 4, showing the difference in both the total and diffuse reflectance of untreated and solvent-treated, additive-free PP samples in the 200–2500 nm wavelength range.

As expected, the untreated extruded PP sheet, which has a smooth surface, only reflects less than 10% of solar irradiance, the lowest value among all the investigated structures. In the 200–2500 nm range, the spectrophotometry results of solvent-treated samples show almost an order of magnitude stronger reflection compared to their untreated counterparts due to the porous layers created. The cooling performance of solar-reflective surfaces is usually characterized with their TSR values. A substantial increase in the reflectance spectra and TSR was observed for the solvent-treated PP samples with increasing immersion times from 60 to 180 s. The change in reflectance is consistent with the structural changes.

The rise in solar reflectance is caused by the increased interface area, which is a consequence of the porous structure. On the other hand, the anisotropic porous structure with broader primary pore size distribution and the micro- and nano-scaled roughened spherulites in the cross-section of the porous structure also improve reflectivity in a wide wavelength range [24]. Also, as X_c increases, the intensity of scattered light also increases, due to the scattering of light at the crystal interfaces [42].

Above 800 nm, in the NIR range, absorption bands are superposed on the spectra, which can be attributed to methylene and methyl overtones and combination bands, characteristic of PP. The absorption bands remain practically the same (determined by the chemical structure), while the physical (scattering) processes determine the shift of the spectra. The differences in the total and diffuse reflectance values amount to a few percent (Fig. 4), because the incident light reflected from the surface is almost entirely reflected diffusely, which can be explained with the surface structure. In the following, only the total reflectance values are used. Solvent-induced recrystallization leads to a restructured, partly porous layer in PP samples (covered by a protective

Table 2 The TSR of PP composites

Mass percent of additives (mass%)	TSR/%	
	$PP/BaSO_4$	PP/TiO_2
0	11.6	
5	28.3	82.0
10	39.3	84.9
20	49.1	86.7

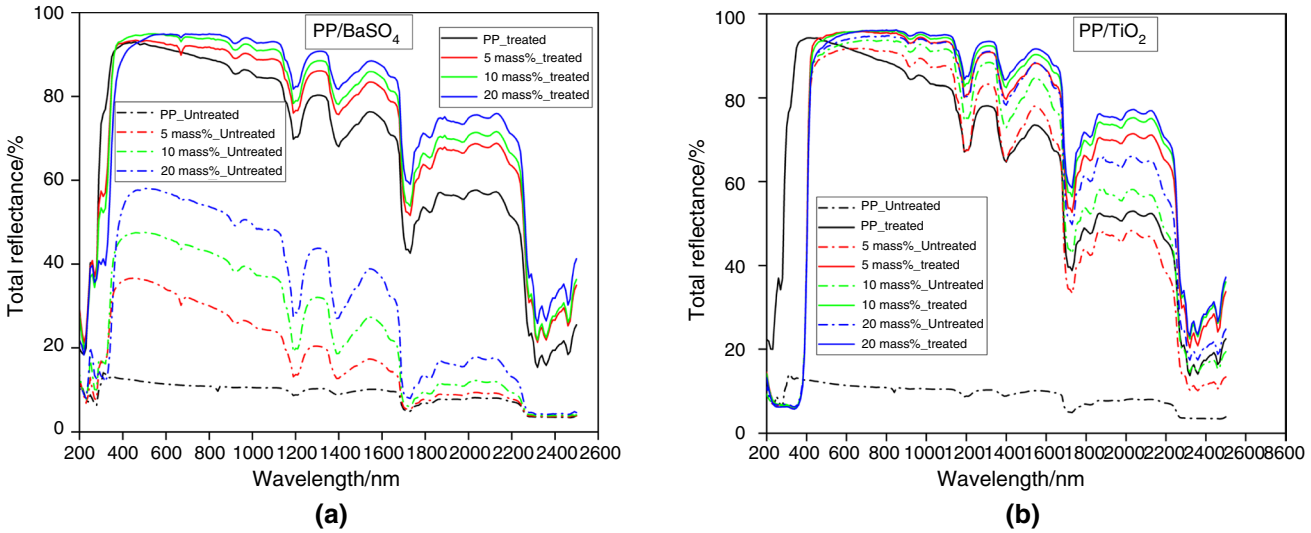

Fig. 6 Total reflectance of **a** $PP/BaSO_4$ samples and **b** PP/TiO_2 samples before (noted as untreated) and after (noted as treated) the solvent treatment. The solvent treatment conditions were: 125 °C, 180 s

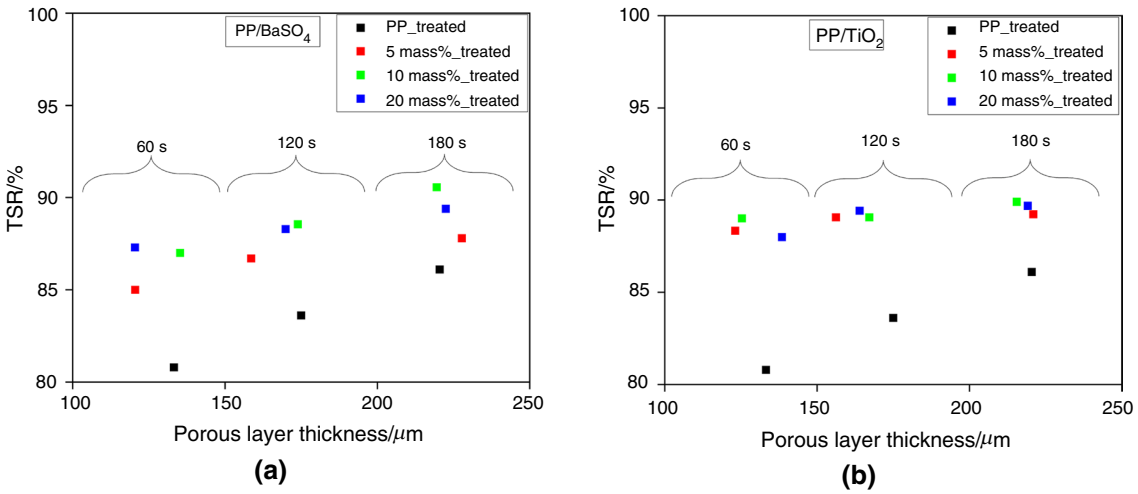

Fig. 7 TSR result of **a** porous PP/$BaSO_4$ samples and **b** porous PP/TiO_2 samples as a function of porous layer thickness. The solvent treatment conditions were 125 °C, 60, 120, and 180 s

skin layer), resulting in an enhanced diffuse reflection in the whole solar spectrum. Incoming light will suffer multiple reflections and be reflected back diffusely as it meets the surface and near-surface of spherulites, which act as independent scattering centers.

Similarly, we investigated the importance of the skin layer on reflectance and indirectly, its effect on passive cooling efficiency—we compared the total reflectance of the solvent-treated samples with and without the skin layer (Fig. 5).

We found that the reflectance of the samples without intact skin layers is slightly higher than that of the unpeeled samples. We concluded that the skin layer is practically transparent and forms a "conformal layer" on the sample surface, therefore it does not influence scattering. Moreover, the skin layer protects the subsurface, so we retained it [26]. Leaving out the peeling process simplifies the manufacturing process and improves the mechanical stability of the product.

By increasing immersion time from 60 to 180 s, TSR increased from 11.0% (untreated PP) to 80.3% (60 s) and 86.1% (180 s). However, while immersion time increased threefold, TSR only increased by 7%. To achieve better solar reflection and thus more effective thermal insulation, we examined two strategies: the combination of a porous structure with reflective additives and the modification of the porous structure with a PP nucleating agent.

Combination of the porous structure with reflective additives

To further improve solar reflection, we distributed TiO_2 and $BaSO_4$ particles in the PP matrix in different amounts (5, 10, and 20 mass%) and solvent-treated the samples at 125 °C for 60, 120, and 180 s. We investigated how the porous PP composite samples composed of a three-dimensional porous structure, and internally distributed reflective additives can enhance solar reflectance.

In Fig. 6a and b, we compare the solar reflectance of PP composites (PP/TiO_2 and PP/$BaSO_4$) before and after the solvent treatment. Only the samples solvent treated for 180 s are plotted in Fig. 6.

In Fig. 6a and b, samples labeled with dash-dot lines represent extruded PP and PP composites before the solvent treatment and the solid lines represent the solvent-treated PP and PP composites. In the case of PP composites, we experienced a different increment in solar reflectance compared to the extruded PP samples depending on the type of additives, as we increased filler content from 5 to 20%. The solar reflectance of PP/$BaSO_4$ composite samples without solvent treatment shows moderate improvement. One possible reason for the moderate reflection performance of PP/$BaSO_4$ composite samples might be the use of single-sized particles of $BaSO_4$ with a particle size too large to effectively scatter such wavelengths. A pleasant surprise is that the solar reflectance of all the PP/TiO_2 composite samples is dramatically higher. As it is known, TiO_2 is a strong UV absorber, thus the PP/TiO_2 composite samples show a sharp drop in the UV range (200 – 400 nm), resulting in a UV reflectance below 10%. However, in the VIS (400–800 nm) and NIR (700 – 2500 nm) wavelength range, reflectance increases significantly with increasing concentration of TiO_2. In the VIS wavelength range, the reflectance of porous PP treated for 180 s is exceeded by the reflectance of PP/TiO_2 composite samples with 5 mass% of TiO_2, which also shows the excellent VIS reflection property of the TiO_2 additive. Above 10 mass% of TiO_2 concentration, PP/TiO_2 samples show better performance in both VIS and NIR light ranges compared to the porous PP sample treated for 180 s. Table 2 shows the TSR values

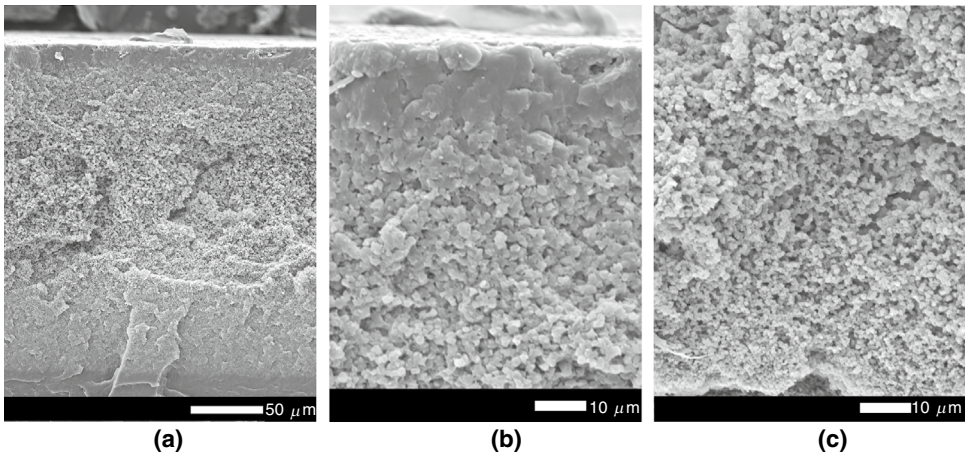

Fig. 8 Cross-sectional SEM image **a** of a porous layer of a nucleated PP sample. SEM image of the magnification of the upper (**b**) and the lower **c** part of the porous layer in (**a**). The applied solvent treatment conditions are 125 °C, 60 s

of extruded PP and PP composites with different reflective additive concentrations.

A comparison of the TSR of extruded PP samples with and without an additive shows that both additives increased TSR considerably but TiO_2 was far more effective. 5 mass% $BaSO_4$ in the PP matrix led to a 2.5 times increase in TSR, and 20 mass% produced an increase in TSR a little over four times. TiO_2 on the other hand, produced a very high TSR even in 5 mass%. (over 7 times more than the neat PP sheet). However, increasing the amount of TiO_2 did not increase TSR much.

The synergistic effect of porous structure and reflective particles results in the enhancement of solar reflection performance. We extended the solar reflection comparison of solvent-treated PP composites with different concentrations of additives and varied the immersion times (60, 120 and 180s). The TSR results of solvent-treated PP composite samples as a function of the thickness of the porous layer can be seen in Fig. 7a and b.

In Fig. 7a and b, the TSR values of porous PP samples (without any additive) with different pore thicknesses are shown with black squares. Porous PP/$BaSO_4$ (TSR: 85.0%) and porous PP/TiO_2 (TSR: 88.3%) samples, both containing minimal amount of additives (5 mass%) and with a brief solvent treatment (60 s), exhibit comparable or even enhanced performance compared to porous PP, solvent treated for 180 s (TSR: 86.1%). This improvement can be attributed to the effective light scattering caused by the additives, as well as the inherent internal pore structure formed by spherulites.

Through increasing additive concentration and solvent immersion time, the solvent-treated PP/$BaSO_4$ composite samples exhibited a gradual rise in TSR values, reaching approximately 90%. This increase was achieved by simultaneously enhancing additive concentration and prolonging immersion time, resulting in an increase in porous layer thickness. Notably, the PP/$BaSO_4$ composite samples containing 10 and 20 mass% $BaSO_4$, with porous layer

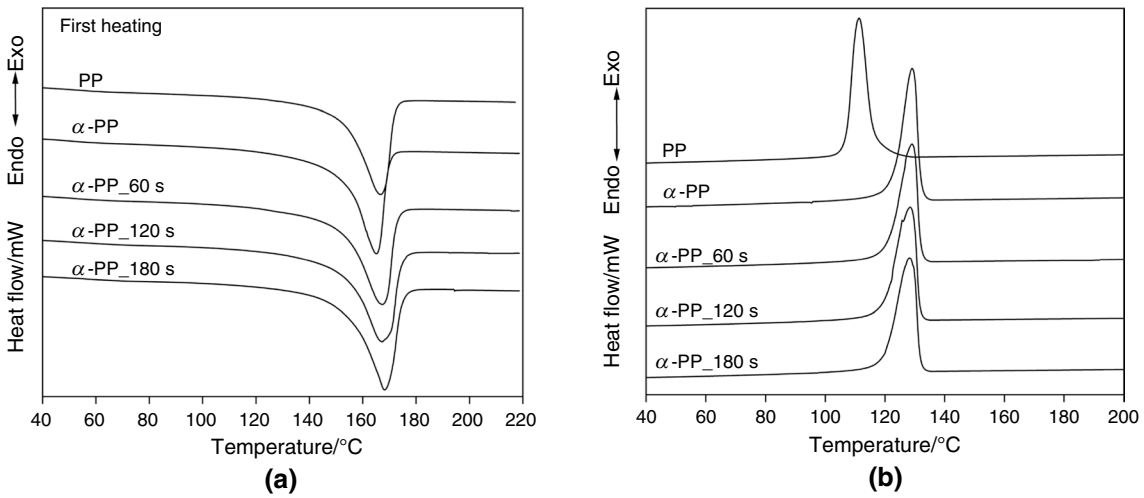

Fig. 9 **a** First melting and **b** crystallization curves of neat PP and nucleated PP and solvent-treated nucleated PP samples

Table 3 Crystalline parameters of the PP, nucleated PP, and solvent-treated nucleated PP

Sample	T_m /°C	T_c /°C	H_m /J g^{-1}	X_c /%*
PP	166.62	112.71	80.52	38.9
α-PP	164.91	128.18	85.28	41.2
α-PP_ 60 s	166.93	129.03	88.59	42.8
α-PP_ 120 s	167.19	128.88	90.87	43.9
α-PP_ 180 s	167.37	128.41	93.34	45.1

*X_c is calculated from the first melting enthalpy

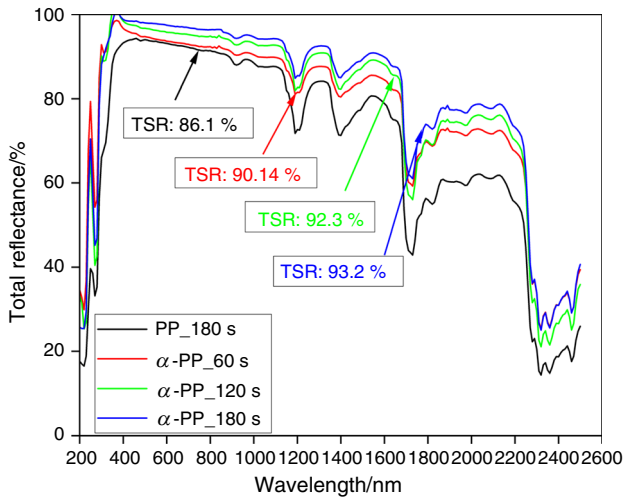

Fig. 10 Solar reflectance of porous nucleated PP samples solvent treated for 60, 120, and 180 s. The TRS values for the spectra are marked with the same color

thicknesses of 219.5 and 222.5 µm, respectively, had a TSR of 90%. These specific layer thicknesses corresponded to a solvent treatment time of 180 s.

In the case of PP/TiO_2 composite samples, increased additive content or solvent treatment time did not increase TSR significantly over the TSR of the sample with the lowest amount of the additive and solvent treated for the shortest time (60 s). The 5 mass% PP/TiO_2 samples prepared with the shortest immersion time (60 s) had a porous layer thickness of 123.1 µm and a TSR of 88.34%. The 10 and 20 mass% PP/TiO_2 samples surface treated for 180 s have porous layer thicknesses of 215.5 and 219.1 µm and a TSR of 89.9% and 89.6%, respectively. A shorter treatment time is preferable for the solvent-treated PP/TiO_2 composite samples since treatment is faster and the thickness of the porous layer of samples treated for 60 s is half that of samples solvent treated for 180 s, resulting in samples with better mechanical properties. Furthermore, the lower content of additives also contributes to reducing the cost of production.

Comparing the solvent-treated and non-solvent-treated PP/$BaSO_4$ and PP/TiO_2 composite samples, we can say that the hierarchical porous surface structure formed on the outer layer of the porous PP/$BaSO_4$ composite samples contributes significantly to the further increase in solar reflectance. In the solvent-treated PP/TiO_2 composite samples, the porous layer contributed to a lesser extent to the increase in the solar reflectance of the untreated samples.

Nonetheless, recent research has highlighted potential environmental and human health concerns related to the utilization of TiO_2 [21]. Moreover, these additives have the potential to considerably increase the overall cost of the final product. Therefore, it becomes imperative to explore substitutes for reflective additive-based systems, taking into account optical performance, as well as environmental and health considerations. Additionally, considering the increasing demand for monomaterial usage to facilitate product recyclability, we also explored nucleated PP samples in conjunction with the PP composites.

Adjusting the porous layer with a nucleating agent

The application of nucleating agents in PP has been well known and used for a long time both in industrial life and in laboratory practice. During the solvent treatment process, the nucleating agents provide more nuclei, so during recrystallization, spherulite growth can start from several points, which results in a decrease in their size. The selected NA 21E nucleating agent was added to PP in a concentration of 500 ppm. Based on previous studies, the recommended amount of NA21E nucleator is around 500 ppm. Above this

Table 4 Comparison of reflectance of various reflective additive-based composites and porous polymers

References	Fabrication method	Reflectance /%
[45]	TiO_2/acrylonitrile-styrene-acrylate copolymer (ASA) hybrid material (volume concentration = 5%)	59.4
[49]	ASA/barium titanate (volume concentration = 1%)	70.0
[48]	Polytetrafluoroethene porous coatings	95.0
[46]	Poly(methyl methacrylate) (PMMA)/chlorinated poly- ethylene (CPE) blending material with porous surface (porosity = 30%)	93.7
[47]	UV irradiated HDPE/ TiO_2 composite	71.2
This work	Porous nucleated PP	93.2

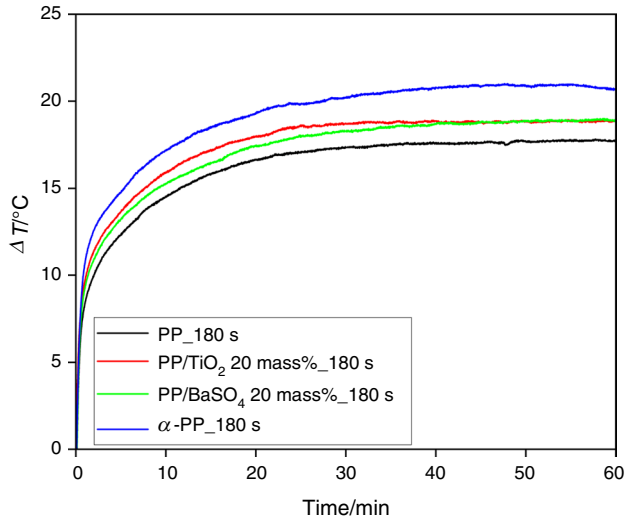

Fig. 11 The temperature difference of porous PP, porous PP composites (with 20 mass% of PP/TiO_2 and $PP/BaSO_4$), and porous nucleated PP samples compared to the extruded PP sheet. The applied solvent treatment time was 180 s

concentration, it becomes saturated [43]. We visualized the cross-sectional morphology of solvent-treated, nucleated PP samples with SEM images, where the porous layer consists of a nano/microporous structure (Fig. 8).

With the application of a nucleating agent, it is possible to effectively reduce the size of the spherulite in the cross-section, thus we can create a more structured porous layer with a larger specific surface area. The diameter of each spherulite is less than 5 µm, and the nucleated PP samples also keep their anisotropic porous structure. The first melting and crystallization curves of PP sample and nucleated PP (α-PP) sample and solvent-treated α-PP samples with different immersion times are shown in Fig. 9. The crystalline parameters of the PP, α-PP, and solvent-treated α-PP samples are shown in Table 3.

For the nucleated PP sample, the crystallization temperature (T_c) increased by 15.5 °C compared to the extruded PP sample and the X_c increased to 41.2%, showing that the nucleation effect of the nucleating agent for the PP is significant. Increasing the solvent treatment time also led to a rise in X_c for the solvent-treated nucleated samples, from 41.2 to 42.8% (60 s), 43.9% (120 s), and 45.1% (180 s). Figure 10 shows the solar spectra of solvent-treated nucleated PP samples, treated for different immersion times, and also the TSR of the individual samples.

The solvent-treated nucleated PP samples treated for 60 s reached a TSR of 90.1%, compared to the 86.1% of porous PP, treated for 180 s. More notably, increasing the immersion time of nucleated PP samples increased TSR to 90.1% (60 s), 92.3% (120 s), and 93.2% (180 s).

Porous nucleated PP samples showed better solar reflectance than porous PP composite samples (without nucleation) regardless of solvent treatment time, presumably due to their increased porosity and specific surface area.

We compared the solar reflectance performance of the porous nucleated PP sample treated for 180 s with that of heat-reflective commercial paints [44, 45] and recently developed light-scattering porous polymer materials [46–49] (Table 4).

As Table 4 shows, the solar reflectance of the porous surface layer in nucleated PP samples (as prepared in this study) surpasses that of additive-based composites. Also, the solar reflectance of the porous nucleated PP samples is nearly identical to that of alternative porous polymer materials.

TSR values are the results of the theoretical calculation of solar spectra, which should also be verified with a cooling test. For this purpose, we performed laboratory-scale simplified sun tests by measuring the temperature inside coated boxes covered with solvent-treated samples and inside a reference box under a sunlight lamp in laboratory conditions. In Fig. 11, we plotted ΔT as a function of time. The samples with the best TSR were selected for the cooling test. The higher the ΔT value, the better heat reflection is.

Based on the trend exhibited by these curves, ΔT curves can be separated into three distinct sections. In the initial 10 min, there is a notable and relatively rapid increase in temperature. Subsequently, between 10 and 40 min, the rise in ΔT follows a progressively diminishing rate. Eventually, in the last 20 min, ΔT stabilizes, reaching an equilibrium phase. The minimum ΔT value belongs to porous PP, solvent treated for 180 s, which can reduce the temperature by around 17 °C compared to the reference sample. 20 mass% porous PP/TiO_2 and 20 mass% porous $PP/BaSO_4$, both solvent treated for 180 s, can reduce the temperature by ~ 19 °C. Nucleated PP solvent treated for 180 s reduced inner surface temperature the most, by ~ 23 °C.

Conclusions

In summary, we proposed a simple solvent treatment method for fabricating a solar reflective, micro- and nanostructured porous PP layer on extruded PP sheets. The thickness of the porous surface layer and its porosity are controlled by the immersion time of the solvent treatment. The solar reflectance of porous PP sheets improves as the thickness of the porous layer and its porosity are increased. The TSR of porous PP sheets with a porous layer thickness of 220.4 µm and 28% porosity is 86.1%. To achieve better solar reflection and thermal insulation

ability, we examined two strategies: (i) the combination of a porous structure and reflective additives ($BaSO_4$, TiO_2) and (ii) the modification of the porous structure with the addition of a PP nucleating agent. A comparison shows that TiO_2 seems to be a more effective additive than $BaSO_4$ in combination with solvent treatment: porous PP/TiO_2 samples show similar TSR values (88.34%, 5 mass%, and 60 s treatment time) to porous PP/$BaSO_4$ samples (TSR: 89.6%, 20 mass%, and 180 s treatment time). Shorter process time and lower additive concentration result in a considerably lower cost of production. When the porosity structure of the samples was improved, the TSR index reached 90.14%. The TSR of nucleated porous nucleated PP samples solvent treated for 60 s was 90.14%, while the TSR of porous nucleated PP samples solvent treated for 180 s reached 93.2%. Cooling performance tests showed that porous PP, porous PP composite (with 10 mass% of PP/TiO_2 and PP/$BaSO4_4$), and porous nucleated PP samples reduced the temperature by 17, 19, and 23 °C, respectively, compared to extruded PP sheets. Cooling tests showed that the porous nucleated PP samples showed the best cooling performance.

The results of solar reflectance and cooling tests indicate that adjusting the porous surface layer on PP sheets with a nucleating agent presents a viable alternative cooling method compared to systems that use electrical energy for cooling.

Author contributions All authors contributed to the study conception and design. Material preparation, data collection and analysis were performed by CV. The first draft of the manuscript was written by CV and all authors commented on previous versions of the manuscript. All authors read and approved the final manuscript.

Funding Open access funding provided by Budapest University of Technology and Economics. Project no.c1781534HAS BEEN IMPLEMENTED WITH THE SUPPORT PROVIDED BY THE MINISTRY OF CULTURE AND INNOVATION OF HUNGARY FROM THE NATIONAL RESEARCH, DEVELOPMENT AND INNOVATION FUND, FINANCED UNDER THEKDP-2021FUNDING SCHEME. PROJECT NO. TKP-6–6/PALY-2021 HAS BEEN IMPLEMENTED WITH THE SUPPORT PROVIDED BY THE MINISTRY OF CULTURE AND INNOVATION OF HUNGARY FROM THE NATIONAL RESEARCH, DEVELOPMENT AND INNOVATION FUND, FINANCED UNDER THE TKP2021-NVA FUNDING SCHEME.

Declarations

Conflict of interest The authors have stated explicitly that there are no conflicts of interest in connection with this article. The authors declare they have no financial interests.

References

1. Silva R, Eggimann S, Fierz L, Fiorentini M, Orehounig K, Baldini L. Opportunities for passive cooling to mitigate the impact of climate change in Switzerland. Build Environ. 2022;208:108574. https://doi.org/10.1016/j.buildenv.2021.108574.
2. Elaouzy Y, El Fadar A. Energy, economic and environmental benefits of integrating passive design strategies into buildings: a review. Renew Sustain Energy Rev. 2022;167:112828. https://doi.org/10.1016/j.rser.2022.112828.
3. Bhamare DK, Rathod MK, Banerjee J. Passive cooling techniques for building and their applicability in different climatic zones—The state of art. Energy Build. 2019;198:467–90. https://doi.org/10.1016/j.enbuild.2019.06.023.
4. Taleb HM. Using passive cooling strategies to improve thermal performance and reduce energy consumption of residential buildings in UAE buildings. Front Arch Res. 2014;3:154–65. https://doi.org/10.1016/j.foar.2014.01.002.
5. Mousavi S, Gijón-Rivera M, Rivera-Solorio C, Rangel CG. Energy, comfort, and environmental assessment of passive techniques integrated into low-energy residential buildings in semi-arid climate. Energy Build. 2022;263:112053. https://doi.org/10.1016/j.enbuild.2022.112053.
6. Levinson R, Berdahl P, Akbari H, Miller W, Joedicke I, Reilly J, Suzuki Y, Vondran M. Methods of creating solar-reflective nonwhite surfaces and their application to residential roofing materials. Sol Energy Mater Sol Cells. 2007;91:304–14. https://doi.org/10.1016/j.solmat.2006.06.062.
7. Mandal J, Fu Y, Overvig AC, Jia M, Sun K, Shi NN, Zhou H, Xiao X, Yu N, Yang Y. Hierarchically porous polymer coatings for highly efficient passive daytime radiative cooling. Science. 2018;362:315–9. https://doi.org/10.1126/science.aat9513.
8. Dong S, Quek JY, Van Herk AM, Jana S. Polymer-encapsulated TiO2 for the improvement of NIR reflectance and total solar reflectance of cool coatings. Ind Eng Chem Res. 2020;59:17901–10. https://doi.org/10.1021/acs.iecr.0c03412.
9. Li X, Peoples J, Yao P, Ruan X. Ultrawhite BaSO4 paints and films for remarkable daytime subambient radiative cooling. ACS Appl Mater Interfaces. 2021;13:21733–9. https://doi.org/10.1021/acsami.1c02368.
10. Rahman T, Nagano K, Togawa J. Study on building surface and indoor temperature reducing effect of the natural meso-porous material to moderate the indoor thermal environment. Energy Build. 2019;191:59–71. https://doi.org/10.1016/j.enbuild.2019.03.014.
11. Yu S, Guo B, Johnsen S, Wiegand G, Lemmer U, Guo X, Zhang M, Li Y, Sprau C, Hölscher H. Nanoporous polymer reflectors for organic solar cells. Energ Technol. 2022;10:2100676. https://doi.org/10.1002/ente.202100676.
12. Rashidi S, Hormozi F, Doranehgard MH. Abilities of porous materials for energy saving in advanced thermal systems. J Therm Anal Calorim. 2021;143:2437–52. https://doi.org/10.1007/s10973-020-09880-9.
13. Peoples J, Li X, Lv Y, Qiu J, Huang Z, Ruan X. A strategy of hierarchical particle sizes in nanoparticle composite for enhancing solar reflection. Int J Heat Mass Transf. 2019;131:487–94. https://doi.org/10.1016/j.ijheatmasstransfer.2018.11.059.

14. Tao Y, Mao Z, Yang Z, Zhang J. Preparation and characterization of polymer matrix passive cooling materials with thermal insulation and solar reflection properties based on porous structure. Energy Build. 2020;225:110361. https://doi.org/10.1016/j.enbuild.2020.110361.
15. Song J, Qin J, Qu J, Song Z, Zhang W, Xue X, Shi Y, Zhang T, Ji W, Zhang R. The effects of particle size distribution on the optical properties of titanium dioxide rutile pigments and their applications in cool non-white coatings. Sol Energy Mater Sol Cells. 2014;130:42–50. https://doi.org/10.1016/j.solmat.2014.06.035.
16. Braun JH, Baidins A, Marganski RE. TiO_2 pigment technology: a review. Prog Org Coat. 1992;20:105–38. https://doi.org/10.1016/0033-0655(92)80001-D.
17. Costa JR, Correia C, Gois JR, Silva SM, Antunes FE, Moniz J, Serra AC, Coelho JF. Efficient dispersion of TiO_2 using tailor made poly (acrylic acid)− based block copolymers, and its incorporation in water based paint formulation. Prog Org Coat. 2017;104:34–42. https://doi.org/10.1016/j.porgcoat.2016.12.006.
18. McNeil L, French R. Multiple scattering from rutile TiO_2 particles. Acta Mater. 2000;48:4571–6. https://doi.org/10.1016/S1359-6454(00)00243-3.
19. Jeevanandam P, Mulukutla R, Phillips M, Chaudhuri S, Erickson L, Klabunde K. Near infrared reflectance properties of metal oxide nanoparticles. J Phys Chem C. 2007;111:1912–8. https://doi.org/10.1021/jp066363o.
20. Veloso RC, Souza A, Maia J, Ramos NMM, Ventura J. Nanomaterials with high solar reflectance as an emerging path towards energy-efficient envelope systems: a review. J Mater Sci. 2021. https://doi.org/10.1007/s10853-021-06560-3.
21. Yu S, Chen J, Gomard G, Hölscher H, Lemmer U. Recent progress in light-scattering porous polymers and their applications. Adv Opt Mater. 2023. https://doi.org/10.1002/adom.202203134.
22. Nallapaneni A, Shawkey MD, Karim A. Specular and diffuse reflectance of phase-separated polymer blend films. Macromol Rapid Commun. 2017;38:1600803. https://doi.org/10.1002/marc.201600803.
23. Zou W, Pattelli L, Guo J, Yang S, Yang M, Zhao N, Xu J, Wiersma DS. Biomimetic polymer film with brilliant brightness using a one-step water vapor-induced phase separation method. Adv Func Mater. 2019;29:1808885. https://doi.org/10.1002/adfm.201808885.
24. Lee SH, Han SM, Han SE. Nanostructure regularity in white beetle scales for stability and strong optical scattering. Opt Mater Exp. 2021;11:1692–704. https://doi.org/10.1364/OME.427047.
25. Yip J, Ng S-P, Wong K. Brilliant whiteness surfaces from electrospun nanofiber webs. Text Res J. 2009;79:771–9. https://doi.org/10.1177/0040517509102797.
26. Syurik J, Siddique RH, Dollmann A, Gomard G, Schneider M, Worgull M, Wiegand G, Hölscher H. Bio-inspired, large scale, highly-scattering films for nanoparticle-alternative white surfaces. Sci Rep. 2017;7:46637. https://doi.org/10.1038/srep46637.
27. Yu S, Fritz B, Johnsen S, Busko D, Richards BS, Hippler M, Wiegand G, Tang Y, Li Z, Lemmer U. Enhanced photoluminescence in quantum dots–porous polymer hybrid films fabricated by microcellular foaming. Adv Opt Mater. 2019;7:1900223. https://doi.org/10.1002/adom.201900223.
28. Syurik J, Jacucci G, Onelli OD, Hölscher H, Vignolini S. Bio-inspired highly scattering networks via polymer phase separation. Adv Func Mater. 2018;28:1706901. https://doi.org/10.1002/adfm.201706901.
29. Donie YJ, Theobald D, Moghadamzadeh S, Mertens A, Hossain IM, Paetzold UW, Lemmer U, Gomard G. Planarized and compact light scattering layers based on disordered titania nanopillars for light extraction in organic light emitting diodes. Adv Opt Mater. 2021;9:2001610. https://doi.org/10.1002/adom.202001610.
30. Yang B, Ding M, Wu J, Chen Q, Zhao H, Yu Y, Pan Y, Qian J, Miao J, Tu Y. In situ tailoring the hierarchical microstructures in polyethylene films fabricated by thermally induced phase separation via temperature gradient fields. J Mater Sci. 2020;55:10922–41. https://doi.org/10.1007/s10853-020-04748-7.
31. Matsuyama H, Yuasa M, Kitamura Y, Teramoto M, Lloyd DR. Structure control of anisotropic and asymmetric polypropylene membrane prepared by thermally induced phase separation. J Membr Sci. 2000;179:91–100. https://doi.org/10.1016/S0376-7388(00)00506-8.
32. Matsuyama H, Berghmans S, Lloyd DR. Formation of anisotropic membranes via thermally induced phase separation. Polymer. 1999;40:2289–301. https://doi.org/10.1016/S0032-3861(98)00040-8.
33. J. Karger-Kocsis, T. Bárány, Polypropylene handbook, Switzerland: Springer Nature, (2019).
34. Mangaraj S, Yadav A, Bal LM, Dash S, Mahanti NK. Application of biodegradable polymers in food packaging industry: A comprehensive review. J Packaging Technol Res. 2019;3:77–96. https://doi.org/10.1007/s41783-018-0049-y.
35. Ma W, Zhou Z, Ismail N, Tocci E, Figoli A, Khayet M, Matsuura T, Cui Z, Tavajohi N. Membrane formation by thermally induced phase separation: Materials, involved parameters, modeling, current efforts and future directions. J Membr Sci. 2022. https://doi.org/10.1016/j.memsci.2022.121303.
36. Luo B, Zhang J, Wang X, Zhou Y, Wen J. Effects of nucleating agents and extractants on the structure of polypropylene microporous membranes via thermally induced phase separation. Desalination. 2006;192:142–50. https://doi.org/10.1016/j.desal.2005.10.013.
37. Vámos C, Rácz I, Bárány T, Menyhárd A, Marosfői BB. Novel, solvent-based method for the production of polymer sheets with a superhydrophobic surface. Polym Eng Sci. 2023;63:1289–302. https://doi.org/10.1002/pen.26283.
38. Vámos C, Varga LJ, Marosfői B, Bárány T. Role of extruded sheet morphology in phase separation and final morphology of superhydrophobic polypropylene, periodica polytechnica. Mech Eng. 2022;66:260–71. https://doi.org/10.3311/PPme.20509.
39. Gee D, Melia T. Thermal properties of melt and solution crystallized isotactic polypropylene. Die Makromolekulare Chemie: Macromol Chem Phys. 1970;132:195–201. https://doi.org/10.1002/macp.1970.021320117.
40. Huang M-C, Xue C-H, Huang J, Liu B-Y, Guo X-J, Bai Z-X, Wei R-X, Wang H-D, Du M-M, Jia S-T. A hierarchically structured self-cleaning energy-free polymer film for daytime radiative cooling. Chem Eng J. 2022;442:136239. https://doi.org/10.1016/j.cej.2022.136239.
41. Kim JF, Kim JH, Lee YM, Drioli E. Thermally induced phase separation and electrospinning methods for emerging membrane applications: a review. AIChE J. 2016;62:461–90. https://doi.org/10.1002/aic.15076.
42. Wang S, Zhang J. Effect of titanium dioxide (TiO_2) on largely improving solar reflectance and cooling property of high density polyethylene (HDPE) by influencing its crystallization behavior. J Alloy Compd. 2014;617:163–9. https://doi.org/10.1016/j.jallcom.2014.07.191.
43. Menyhárd A, Bredács M, Simon G, Horváth Z. Determination of nucleus density in semicrystalline polymers from nonisothermal crystallization curves. Macromolecules. 2015;48:2561–9. https://doi.org/10.1021/acs.macromol.5b00275.
44. Berdahl P, Bretz SE. Preliminary survey of the solar reflectance of cool roofing materials. Energy Build. 1997;25:149–58. https://doi.org/10.1016/S0378-7788(96)01004-3.
45. Qi Y, Xiang B, Zhang J. Effect of titanium dioxide (TiO2) with different crystal forms and surface modifications on cooling property and surface wettability of cool roofing materials. Sol Energy

Mater Sol Cells. 2017;172:34–43. https://doi.org/10.1016/j.solmat.2017.07.017.
46. Mao Z, Qi Y, Yang Z, Jiang G, Zhang J. Fabrication of solar-reflective, hydrophobic polymer materials with excellent cooling and anti-icing properties through selective etching. Appl Surf Sci. 2020;518: 146209. https://doi.org/10.1016/j.apsusc.2020.146209.
47. Wang S, Zhang J, Liu L, Yang F, Zhang Y. Evaluation of cooling property of high density polyethylene (HDPE)/titanium dioxide (TiO2) composites after accelerated ultraviolet (UV) irradiation. Sol Energy Mater Sol Cells. 2015;143:120–7. https://doi.org/10.1016/j.solmat.2015.06.032.
48. Mandal J, Jia M, Overvig A, Fu Y, Che E, Yu N, Yang Y. Porous polymers with switchable optical transmittance for optical and thermal regulation. Joule. 2019;3:3088–99. https://doi.org/10.1016/j.joule.2019.09.016.
49. Xiang B, Zhang J. A new member of solar heat-reflective pigments: $BaTiO_3$ and its effect on the cooling properties of ASA (acrylonitrile-styrene-acrylate copolymer). Sol Energy Mater Sol Cells. 2018;180:67–75. https://doi.org/10.1016/j.solmat.2018.02.027.